Surface relaxation, surface reconstruction and surface dynamics close to the antiferrodistortive phase transition of $SrTiO_3$(001) slabs with free SrO and TiO_2 surfaces

1993 J. Phys.: Condens. Matter 5 1

(http://iopscience.iop.org/0953-8984/5/1/003)

J. Phys.: Condens. Matter 5 (1993) 1–12. Printed in the UK

Surface relaxation, surface reconstruction and surface dynamics close to the antiferrodistortive phase transition of $SrTiO_3(001)$ slabs with free SrO and TiO_2 surfaces

J Prade†||, U Schröder†, W Kress‡, F W de Wette§ and A D Kulkarni§

† Universität Regensburg, D-8400 Regensburg, Federal Republic of Germany
‡ Max-Planck-Institut für Festkörperforschung, D-7000 Stuttgart 80, Federal Republic of Germany
§ Department of Physics, University of Texas, Austin, Texas 78712-1081, USA

Received 17 June 1992

Abstract. We discuss the relaxation, reconstruction and dynamics of both (001) surfaces of $SrTiO_3$ (SrO and TiO_2 surfaces) in the framework of shell models. The treatment of the SrO surface (surface I) on the basis of a bulk shell model leads to relaxation- and surface-dynamical results, the former of which are in good agreement with recent LEED measurements. However, for the TiO_2 surface (surface II), surface-related changes in the Ti–O short-range interactions have to be introduced in the model in order to obtain agreement with the LEED results, as well as to assure dynamical stability of this surface. The physical reason for these model-changes is that the TiO_2 surface truncates the Ti–O octahedra, which results in an electron redistribution at the surface. Both surfaces exhibit soft-mode behaviour which, upon lowering the temperature, leads to surface reconstruction that takes place prior to the antiferrodistortive transition of the bulk.

1. Introduction

Perovskite-structure compounds (perovskites for short) have attracted considerable interest during recent decades because of fundamental as well as technological reasons (Lines and Glass 1977). The fundamental interest is mainly concerned with structural instabilities of the relatively simple perovskite lattice which exhibits cubic symmetry in the high-temperature phase and in this phase contains only one formula unit in the unit cell. In most perovskites the structural instabilities manifest themselves in a series of phase transitions which may be of first- or second-order. The second-order transitions may be driven by a soft phonon mode (displacive phase transition) or by a soft diffusive mode (order–disorder transition). Some of the phase transitions which occur in perovskites are purely structural while others are linked to additional phenomena, such as the occurrence of ferroelectricity, which occurs in a number of perovskites.

Technological interest in perovskites is mainly concerned with their dielectric behaviour.

|| Present address: Siemens AG, Munich, Federal Republic of Germany.

0953-8984/93/010001+12$07.50

(i) The softening of the ferroelectric mode is due to long-range dipolar forces which drive the ferroelectric phase transition. As the ferroelectric transition is approached the dielectric constant ϵ_0 increases and becomes singular at the transition. Perovskites can thus provide very large dielectric constants with substantial non-linear contributions. These non-linearities are employed in optical devices for generation of second harmonics, for electro-optic modulation, as well as in parametric oscillators.

(ii) The direction of the ferroelectric orientation can be used for storage of information.

(iii) Quite recently, additional interest has been generated by the fact that a number of the oxidic perovskites are the parent materials of high-T_c superconductors and some of these (such as $SrTiO_3$) are used as substrate materials for the deposition of epitaxial thin films of high-T_c materials.

In this paper we focus on $SrTiO_3$, which may be called an incipient ferroelectric since it behaves in its high-temperature phase like a ferroelectric in its paraelectric phase. However, the lowest transverse optic mode at the Γ-point of the bulk Brillouin zone (which in actual ferroelectrics drives the ferroelectric phase transition), is not the only low-frequency vibration which softens with decreasing temperature. $SrTiO_3$ exhibits, in addition to this 'ferroelectric soft mode' Γ_{15}, a whole series of low frequency vibrations, which show a pronounced softening with decreasing temperature. The wave vectors of these modes are located at the zone boundary along the line connecting the R-point with the M-point of the Brillouin zone. Upon lowering the temperature, it is in fact the R_{25}-mode and not the ferroelectric mode Γ_{15} that reaches zero frequency first. As a result a displacive phase transition to an antiferrodistortive phase, characterized by the freezing of counter-rotations of neighbouring oxygen octahedra around an O–Sr–O axis, takes place at $T = 105$ K, instead of ferroelectric ordering at about 40 K, as would follow from an extrapolation of the high-temperature behaviour of the dielectric constant by a Curie–Weiss law. The ferroelectric phase is in fact never reached in $SrTiO_3$ since the dielectric constant shows deviations from a simple Curie-Weiss law and increases monotonically to lowest temperatures without reaching a singularity.

It should be mentioned in passing that when a small amount of oxygen is removed from the lattice, $SrTiO_3$ becomes semiconducting and free electron carriers are produced. Both the ferroelectric mode and the antiferrodistortive mode are very sensitive to the concentration of oxygen vacancies (Wagner *et al* 1980, Bäuerle *et al* 1980, Bussmann-Holder *et al* 1981).

In the present paper we are mainly concerned with the following questions.

(i) How does the (100) surface of the high-temperature cubic phase of $SrTiO_3$ relax on cleavage and what is the temperature dependence of the relaxation pattern?

(ii) Are there surface localized modes which correspond to the antiferrodistortive bulk modes and what is their temperature dependence?

(iii) Are there soft surface modes and does the freezing of these modes lead to a surface reconstruction prior to the antidistortive transition of the bulk?

In the following sections we will try to shed some light on these questions. In section 2, we present the lattice dynamical model on which our investigation is based. Applying this model to the static case, we calculate in section 3 the relaxation pattern of both the SrO and the TiO_2 (100) surfaces of the high-temperature phase. In section 4 we investigate the dynamics of the relaxed surfaces. Section 5 is devoted to

the temperature dependence of surface modes and of relaxation. Finally, a summary and conclusions are given in section 6.

2. Foundations

The bulk phonons of $SrTiO_3$ have been investigated quite extensively by inelastic neutron scattering measurements (Cowley 1964, Yamada and Shirane 1969, Shirane and Yamada 1969, Cowley *et al* 1969, Stirling 1972, Stirling and Currat 1976). The measured phonon dispersion curves are well reproduced by various shell-model calculations (Bussmann-Holder *et al* 1981, Cowley 1964, Stirling 1972, Migoni *et al* 1976, Cowley 1978) which take into account long-range Coulomb interactions between the ions, short-range repulsive forces, and displacement-induced deformations of the electronic charge densities in the dipole approximation.

Unfortunately, as they are, these models are not well suited for the calculation of surface dynamics and relaxation since the short-range interactions are represented by force constants. These force constants, which are obtained from fitting to the measured bulk dispersion curves, can be considered as the derivatives at the bulk equilibrium positions of otherwise unspecified potentials. By the formation of a surface the bulk symmetry is broken so that the net forces acting on cores and shells of ions at and close to (i.e. near) the surface are different from those in the bulk, even when the interaction potentials between particles in the bulk and at the surface are the same. Consequently, in general, cores and shells of ions near the surface move into new equilibrium positions which are slightly different from those of the bulk. Thus, the forces acting at these new equilibrium positions near the surface are different from those of the bulk and they can be calculated only if the potentials (not just the force constants) of the interactions are known. It is therefore necessary to specify the functional form of interaction potentials and to determine the parameters of these potentials in such a way that the bulk dispersion curves are reproduced by calculations based on these potentials.

$SrTiO_3$ is a predominantly ionic crystal. We can therefore assume that, in contrast to the case of metals and homopolar compounds, there is no major rearrangement of the electronic states near the surface, and that the interaction potential is essentially made up of two-body contributions which do not depend on the environment of the interacting ions†. Incidentally, it has been precisely this idea of configuration independent interactions which enabled us to present a full analysis of the optical spectra of high-T_c materials (which in fact show strong structural similarities with perovskites) on the basis of essentially little more than the structural data of these compounds(Prade *et al* 1987, Kress *et al* 1988, Prade *et al* 1989, Kulkarni *et al* 1989, Kress *et al* 1989, Kulkarni *et al* 1990, Heyen *et al* 1990).

† There exist small deviations from the Cauchy relation $c_{12} = c_{44}$, which indicate that many-body contributions are not completely absent. These contributions are, however, much smaller than the two-body contributions and have only minor effects on the dispersion curves in the bulk. In going from the bulk to the surface, the many-body contributions may change drastically. Nonetheless they remain small compared to the two-body contributions. These many-body contributions at the surface can in principle be obtained either from first-principles calculations, which are however not feasible at present, or from the measured surface phonon dispersion curves, which are not yet available for $SrTiO_3$. We therefore postpone the refinement of our treatment until more data become available. We expect, however, that our present calculations predict the main features of the surface dynamics quite well.

Thus, as a first step in our analysis we have to determine the interaction potentials. For the Coulomb interactions we know already the potential

$$V(r_{ij}) = \frac{Z_i Z_j}{|r_j - r_i|}. \tag{1}$$

For the surface calculations we have to impose some restrictions on the ionic charges which go slightly beyond the charge neutrality required in the bulk. Since we are interested in a slab with free (100) surfaces, we have to require charge neutrality for the individual SrO and TiO_2 layers of which the slab is formed and with which it terminates. Otherwise the slab either would not be electrically neutral or would have a residual dipole moment. With integer ionic charges this condition is automatically fulfilled. However, shell models normally allow for a small charge transfer which reduces the full ionic charges by a few per cent. The combined conditions of overall and layer-wise charge neutrality of the slab are expressed by

$$Z_{Sr} = -Z_O$$

$$Z_{Ti} = -2Z_O. \tag{2}$$

For the short-range overlap repulsive interactions, we assume Born–Mayer potentials of the form:

$$V_{ij}(r) = a_{ij} \exp(-b_{ij} r). \tag{3}$$

The longitudinal force constants A_{ij} and the transverse force constants B_{ij} are then given by

$$A_{ij}\left(\frac{e^2}{2v_a}\right) = \frac{\partial^2}{\partial r^2} V_{ij}(r)\bigg|_{r=r_{ij}^0}$$

$$B_{ij}\left(\frac{e^2}{2v_a}\right) = \frac{1}{r}\frac{\partial}{\partial r} V_{ij}(r)\bigg|_{r=r_{ij}^0} \tag{4}$$

where e is the electronic charge, v_a the volume of the unit cell, and r_{ij}^0 the equilibrium distance of ions i and j. For Born–Mayer potentials, (4) implies that

$$\frac{A_{ij}}{|A_{ij}|} = -\frac{B_{ij}}{|B_{ij}|}. \tag{5}$$

This is a further constraint that has to be satisfied in the fitting procedure to obtain the potential parameters a_{ij} and b_{ij}. The first derivatives of the potentials have to fulfill the equilibrium condition in the bulk

$$4\alpha_M + 12(B_{Sr-O} + B_{O-O}) + 3B_{Ti-O} = 0 \tag{6}$$

where α_M is the Madelung constant.

The free-ion polarizabilities are determined by the intra-ionic core-shell force constants k_i and the shell charges Y_i. Unfortunately, the functional form of the potential underlying k_i is not known. However, it is reasonable to assume that for those ions which are stable in the free state, the changes in polarizability induced by variations in the arrangement of the surrounding ions are taken into account by the variation of the coupling to these surrounding ions and not by a change in the intra-ionic interaction. For stable ions, we therefore treat Y_i and k_i as configuration-independent constants.

Oxygen deserves special attention since the O^{2-} ion is not stable in the free state so that the Coulomb field of the surrounding ions in a solid is needed for the stabilization of the O^{2-} ion. As a consequence, the oxygen polarizability depends strongly on the arrangement of the local environment of the ion (Bussmann *et al* 1980) and, for example, varies strongly when the local environment is modulated by a phonon. For instance, oxides show extremely strong Raman intensities for modes which involve displacements of oxygen ions relative to their local environment, since the matrix element for Raman scattering is proportional to the derivative of the polarizability with respect to the phonon normal coordinate. Because of the drastic change in the ionic environment at the surface, we expect changes in the core-shell on-site force constant k_O of the surface O^{2-} ions. At present the only way to deal with these changes is to fit the force constant k_O for the O^{2-} ions at the surface to measured surface properties. Unfortunately, the data on $SrTiO_3$ surfaces are very limited at present. In particular, data for the optical surface modes which depend strongly on the electronic polarizability are completely lacking.

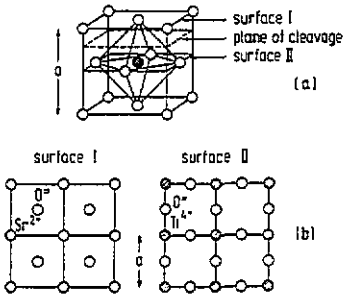

Figure 1. (*a*) Perovskite unit cell and (001) plane of cleavage. (*b*) Geometries of SrO and TiO_2 surfaces (surfaces I and II, respectively).

Table 1. Bulk shell model for $SrTiO_3$. Model II of Becher (1989).

Shell parameters				
Ion	$Z(\|e\|)$	$Y(\|e\|)$	$k_{\parallel}(e^2/v_a)$	$k_{\perp}(e^2/v_a)$
Sr	1.75	2.120	73.0	73.0
Ti	3.50	−13.995	33957.6	33957.6
O	−1.75	−2.625	179.1	384.4
Born–Mayer potentials				
	$a(eV)$	$b(Å^{-1})$	$A(e^2/v_a)$	$B(e^2/v_a)$
Sr–O	3864.1	3.532	23.148	−2.377
Ti–O	1083.0	2.994	232.445	−39.756
O–O	99829.0	5.600	4.951	−0.320

The cleaving of a $SrTiO_3$ crystal perpendicular to a [001] direction creates two (001) surfaces, namely a SrO surface (surface I) and a TiO_2 surface (surface II) (cf figure 1). Since the formation of surface I does not cut the TiO_6 octahedra, we expect smaller changes in the O^{2-} polarizability for surface I than for surface II. These changes in the electronic polarizability will strongly influence the behaviour of the 'ferroelectric surface mode' which is peeled down from the transverse optic bulk band at the centre of the Brillouin zone. At present we are unable to adjust k_O properly at the surface; therefore, we take the unmodified bulk values. For the present study this is, however, not crucial since we are primarily interested in the antiferrodistortive soft mode which depends essentially on the difference between Coulomb and short-range terms and not so much on the electronic polarizability changes at the surface. We base our study on a recent reinvestigation of the measured phonon dispersion curves in the bulk (Becher 1989). In this work a shell model was used which fulfilled all the constraints given above. The parameters of this model are shown in table 1.

3. Surface relaxation

While the bulk properties of perovskites have been extensively investigated (Lines and Glass 1977, Bilz and Kress 1979), the study of their surface properties has become feasible only quite recently (Bickel *et al* 1989, Toennies and Vollmer 1991). Bickel *et al* (1989) have reported LEED measurements of the structure of the (100) surfaces of $SrTiO_3$. These measurements stimulated us to extend our earlier calculations of the structure and dynamics of the (100) surfaces of the fluoridic perovskites $KZnF_3$ and $KMnF_3$ (Prade *et al* 1988, Reiger *et al* 1989) to the oxidic perovskite $SrTiO_3$, (Prade *et al* 1990, Schröder *et al* 1990) which shows similar soft-mode behaviour in the bulk. As is shown in figure 1, a (100) slab of $SrTiO_3$ can either terminate with a SrO or a TiO_2 surface. The experimental results (Bickel *et al* 1989) show that in fact both surfaces occur in nature. A comparison of our initial results (Schröder *et al* 1990) with the LEED data (Bickel *et al* 1989) showed good agreement for the SrO surface while the results for the TiO_2 surface were not at all satisfactory.

In our calculation of the surface relaxation we follow closely the procedure described in Reiger *et al* (1989) for $KZnF_3$ and $KMnF_3$. All considerations and comments given there apply equally to $SrTiO_3$ and will not be repeated here. In the following, we therefore concentrate on the presentation and discussion of the results for both the SrO (surface I) and the TiO_2 surface (surface II).

3.1. Surface I

The SrO surface shows a strong similarity to the (100) surfaces of alkali halides for which we have shown in earlier work that both surface relaxation (de Wette *et al* 1985, 1987) and the dynamics of the relaxed surfaces (Kress *et al* 1987) can be appropriately treated in the framework of shell models based on interaction potentials derived from bulk properties. Hybridization between the d-orbitals of the transition metal Ti and the p-orbitals of oxygen plays an important role in the stability of the oxygen octahedra, which can be viewed as the backbone of the perovskite structure. This is evident, for instance, in the case of $LiNbO_3$ (Birnie 1990). In that case the small Li ions arrange themselves in various ways in the voids of the structure, leaving the network of the octahedra unchanged. The formation of the SrO surface leaves

the local coordination of the Ti ions at the centres of the topmost oxygen octahedra unaffected. We therefore anticipate that the formation of this surface does not cause any major changes which are not taken into account in our relaxation procedure as described above.

Table 2. Comparison of calculated and measured values of the changes of interlayer distances $\Delta d_{ij}/d_0$ and surface rumpling r. d_0 represents the bulk distance, $\Delta d_{ij} = d_{ij} - d_0$, $r = z(O^{2-}) - z(Sr^{2+}(Ti^{4+}))$. Calculation with the parameters given in table 1.

	Surface I		Surface II	
	Calculated	Experiment[a]	Calculated	Experiment[a]
r(Å)	0.179	0.16(±0.08)	0.047	0.08(±0.08)
$\Delta d_{12}/d_0$(%)	−9.5	−10(±2)	−7.9	2(±2)
$\Delta d_{23}/d_0$(%)	2.9	4(±2)	2.4	−2(±2)

[a] Bickel *et al* 1989.

The calculated values of the relative changes in the interlayer distance $\Delta d_{ij}/d_0$, where d_0 is the bulk distance between adjacent layers, and the surface rumpling r, compare quite well with the measured values (Bickel *et al* 1989) as can be seen from table 2. In figure 2 we present a side view of the relaxation pattern of surface I. We mention that the shell radii drawn in the figure are arbitrary and do not have any physical meaning; they do not represent the spatial extent of the electronic charge distributions. The variables of the shell model are only the core positions and the relative displacements of the shell centres with respect to the core positions. In the bulk, these relative displacements vanish in the static case because of symmetry. At the surface, however, static dipoles are formed by the relaxation. The formation of these dipoles is real and is a consequence of the lowered symmetry at the surface. As expected, the relaxation pattern is very similar to that of the (100) surfaces of the alkali halides (de Wette *et al* 1985, 1987); the interplanar distance d_{12} between the first and the second layer is diminished while the interplanar distance d_{23} is increased with respect to d_0. At the surface the Sr^{2+} ions move inward with respect to the average surface plane while the O^{2-} ions move outward.

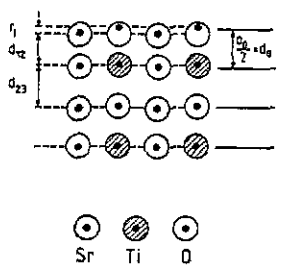

Figure 2. Relaxation pattern of the SrO surface (surface I) of $SrTiO_3$, viewed along the [010] direction. The displacements in the z-direction are enhanced by a factor of two.

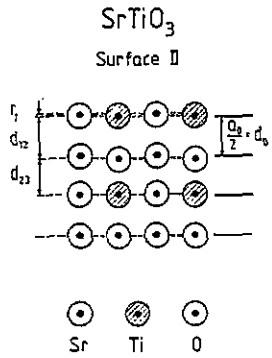

Figure 3. Relaxation pattern of the TiO_2 surface (surface II) of $SrTiO_3$, viewed along the [010] direction. The displacements in the z-direction are enhanced by a factor of two.

3.2. Surface II

Surface II is the TiO_2 surface. By the formation of this surface the coordination of the Ti ion at the centre of the topmost oxygen tetrahedra is changed by cutting away the optical oxygens. Thus, we anticipate major changes in the interactions due to a rearrangement of the electronic states at the surface. Our initial calculations, which were based on the interactions deduced from the bulk data, did not allow for these changes. As can be seen from table 2, the initial model gives quite unsatisfactory agreement with the experimental data for this surface. Moreover, it yields dynamical instabilities at the surface (i.e. imaginary surface phonon frequencies). In order to overcome the inherent limitations of this procedure, we have to include in our considerations the changes of the electronic system near the surface. Since we did not carry out a direct calculation of the interaction potentials from a full analysis of the electronic ground state energy as a function of the ionic displacements, we have as a minimum to account for these near-surface changes in the short-range interaction potentials and the electronic polarizabilities, by determining these quantities empirically from the experimental data. In the present investigation it was sufficient to take into account the increased overlap between the Ti^{4+} ion at the surface and its surrounding five O^{2-} ions (see figure 1(*a*)) in the form of an enhancement of the prefactor $a^{(1)}_{Ti-O}$ to 1.22 $a^{(bulk)}_{Ti-O}$ (the superscript (1) refers to the surface layer). At the same time the prefactor for the interaction of the oxygen in second layer with the titanium in the third layer had to be reduced to $a^{(2)}_{Ti-O} = 0.95 a^{(bulk)}_{Ti-O}$. With these changes the experimental data are reproduced by the the calculations, as can be seen from table 3. The relaxation pattern for surface II, shown in figure 3, is qualitatively different from that of the alkali halides and from that of surface I, since it shows an increase in the distance d_{12} between the first and second layers and a decrease in the distance between the second and third layers while the alkali halides always show inward relaxation of the first layer.

Table 3. Comparison of calculated and measured values of the changes of interlayer distances $\Delta d_{ij}/d_0$ and surface rumpling r of surface II. d_0 represents the bulk distance, $\Delta d_{ij} = d_{ij} - d_0$, $r = z(O^{2-}) - z(Sr^{2+})$

	Surface II	
	Calculated	Experiment[a]
r(Å)	0.032	0.08(±0.08)
$\Delta d_{12}/d_0$(%)	1.2	2(±2)
$\Delta d_{23}/d_0$(%)	−1.5	−2(±2)

[a] Bickel *et al* 1989.

4. Dynamics of the relaxed surfaces

Up to this point we have been concerned with the static properties. We now discuss the dynamical effects. Both the static and the dynamical properties involve the same interactions. We are thus confident that the interaction potentials with which we achieved quite a good agreement between the calculated and the measured relaxation pattern, can also serve as a reliable basis for the calculation of the surface vibrations

of both the SrO and the TiO_2 surfaces. We use the slab method and follow closely the procedure adopted in our analysis of the surface modes of $KZnF_3$ and $KMnF_3$ (Reiger *et al* 1989). We refer to this paper for an extensive discussion of the vibrational character and the classification of the perovskite (100) surface modes; this discussion applies equally well to the $SrTiO_3$ (100) surfaces and will therefore not be repeated here.

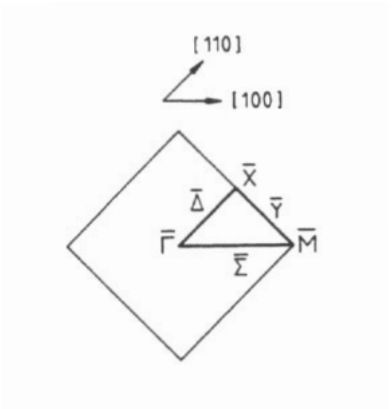

Figure 4. Surface Brillouin zone of the perovskite (001) slab.

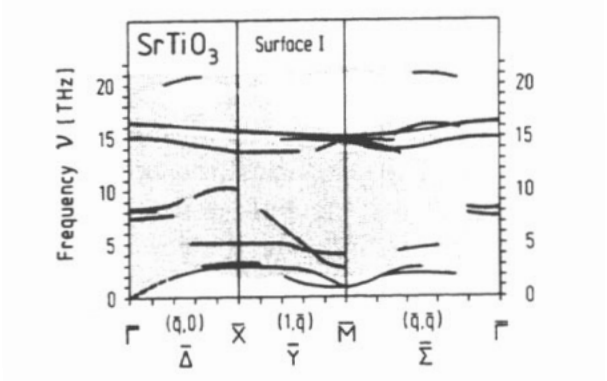

Figure 5. Surface-mode dispersion curves for the SrO surface (surface I) of $SrTiO_3$. The shaded areas represent the bulk bands.

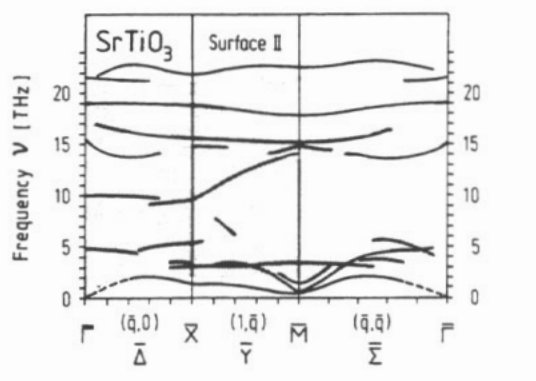

Figure 6. Surface-mode dispersion curves for the TiO_2 surface (surface II) of $SrTiO_3$. The shaded areas represent the bulk bands.

The surface modes are calculated for relaxed 25-layer slabs bounded by either two free SrO or two free TiO_2 surfaces. The room temperature results for surfaces I and II, for wave vectors along the main symmetry directions of the surface Brillouin zone (SBZ) (see figure 4), are shown in figures 5 and 6, respectively. The surface-localized modes are indicated by bold lines while the surface projected bulk vibrations are indicated by the shaded bands. The surface modes exhibit the same characteristics as those of the corresponding surfaces of $KZnF_3$ and $KMnF_3$ (Reiger *et al* 1989) . Of particular interest are the low-frequency surface modes at the $\bar{M}$ point. These modes are peeled down from the lowest bulk band which, at $\bar{M}$, is just the surface projection of the lowest frequency modes along the zone boundary of the bulk Brillouin zone between the R and the M points. These modes are thus strongly related to the soft mode R_{25} which drives the bulk into the antiferrodistortive phase. In the next section we will discuss its vibrational character and its temperature dependence in more detail. Here we only mention that this mode is triply degenerate and that, in the case of surface I, its eigenvectors indicate a complicated motion of the uppermost oxygen octahedra, similar to the corresponding motion of the fluorine octahedra in

$KMnF_3$. It is interesting to note that in $SrTiO_3$ both surfaces show surface-localized low-frequency modes at the $\overline{M}$ point, while such modes are missing for the MnF_2 surface (surface II) of $KMnF_3$. Their appearance in $SrTiO_3$ is due to the stiffening of the TiO_5 clusters, which are remainders of the oxygen octahedra after the oxygen ions at top, together with the surrounding Sr ions, have been cleaved off. The vibrations which involve essentially motions of these clusters as a whole, decouple from the bulk modes in a way similar to the decoupling of the motion of the TiO_6 octahedra at surface I. Further, the stiffening of the Ti–O interactions drives the highest optic modes much higher above the upper bulk band than in $KMnF_3$ and $KZnF_3$, where these modes are essentially located at the upper band edge of the highest optic band. In all these cases the highest surface mode is a sagittal plane mode with predominantly longitudinal optical character. Since this mode does not show up at surface I, an experimental detection of this mode would provide additional proof for the existence of surface II. Moreover, its position above the optic bulk band could possibly be used to determine the oxygen polarizability at the surface. All other surface modes are very similar to those of $KZnF_3$ and $KMnF_3$. We therefore refer to (Reiger *et al* 1989) for further discussion.

5. Temperature dependence of the soft surface modes and surface reconstruction

It has already been mentioned briefly in section 1 that $SrTiO_3$ has two types of modes which can give rise to phase transitions: the lowest frequency transverse optic Γ_{15} mode, which drives the bulk towards the ferroelectric phase transition and the lowest frequency transverse acoustic R_{25} mode which drives the bulk towards the antiferrodistortive transition. The temperature dependence of the ferroelectric soft mode in perovskites can in general be well reproduced by shell models which take into account the lowest order anharmonic term of the on-site core-shell coupling of the oxygen ions (k_O) in the mean field approximation (Bussmann-Holder *et al* 1981, Migoni *et al* 1976).

For the transverse acoustic zone boundary mode R_{25} the situation is more complex. As we have already seen, the frequency of this mode is essentially determined by a small difference of two large terms: a Coulomb contribution and a short-range repulsive contribution. Thus, a slight renormalization by rather small anharmonic short-range contributions drives the system into the antiferrodistortive phase. A full anharmonic calculation of the temperature dependence of the antiferrodistortive soft mode will have to take into account at least the lowest order diagrams for the third and fourth order inter-ionic anharmonic interactions. Since we are here not primarily interested in a calculation of the temperature dependence of the antiferrodistortive bulk phonons, we describe these phonons in the renormalized harmonic approximation by means of temperature dependent force constants, which can in principle be calculated using the above mentioned perturbation theory. We obtain these force constants as derivatives of Born–Mayer functions (3) with temperature-dependent parameters, which in turn are obtained from fits to the measured bulk phonon dispersion curves at various temperatures. It turns out that only two temperature-dependent parameters, namely k_O and A_{Sr-O}, are needed to reproduce the temperature dependence of the dispersion curves from room temperature down to the antiferrodistortive phase transition. The core-shell on-site coupling constant k_O governs essentially the softening of the ferroelectric

mode, while the temperature dependence of the antiferrodistortive soft mode is essentially due to the temperature dependence of the radial force constant A_{Sr-O} of the Sr–O coupling. Figure 7 shows the dependence of the squared frequency $\nu^2_{R_{25}}(T)$ of the antiferrodistortive soft bulk mode on this force constant. The corresponding temperatures can be taken from the experimental data. The upper curve is the bulk curve. It reaches zero frequency at $T_c = 105$ K and thus yields $A_1(105\text{K}) = 22.48e^2/2v_a$. For other temperatures the values of A_1 can be calibrated accordingly, using the measured $\nu^2_{R_{25}}(T)$ relation of the bulk. At each temperature we can now use the appropriate Born–Mayer parameters to calculate the soft surface mode for the properly relaxed slab at the $\overline{M}$ point. In this way we obtain the two lower curves labelled surface I and surface II.

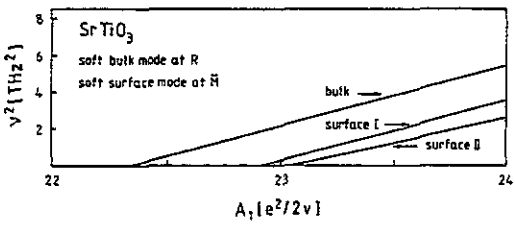

Figure 7. Squared frequency $\nu^2_{R_{25}}(T)$ of the antidistortive bulk soft mode versus the radial force constant A_{Sr-O} of the Sr–O coupling.

It can be seen that the bulk is more stable than the surface, reaching the phase transition after the surface has already undergone reconstruction. It is also interesting to note that the TiO_2 surface (surface II) undergoes the reconstruction at slightly higher temperatures than the SrO surface (surface I); the latter is obviously more stable since the oxygen octahedra remain complete when the surface is formed. The displacement pattern of the reconstruction resembles that of the R_{25} mode in the bulk. It involves counter rotations of neighbouring oxygen octahedra.

6. Summary and conclusions

We have shown that the measured surface relaxation pattern of both the SrO and the TiO_2 surfaces of $SrTiO_3$ can be reproduced by shell-model calculations which are based on interaction potentials deduced from the analysis of the bulk dispersion curves. The relaxation pattern for the SrO surface is obtained without any changes of the interaction potentials. Our results for the TiO_2 surface indicate, however, that for this surface changes in the interaction potentials do occur close to the surface. We conclude from this that the Ti–O interaction is very sensitive to the local coordination of the Ti ions and we attribute this to hybridization. Our calculations indicate that a surface reconstruction occurs for both surfaces prior to the bulk transition, that the order parameter for these transition is in both cases a soft surface phonon and that the reconstruction pattern shows strong similarities with that of the displacive bulk transition.

We hope that this work will stimulate further experimental verification of our results by direct measurements of the surface phonon dispersion curves in general, and of the temperature dependence of the soft surface modes in particular.

In closing we would like to point out that the difference between the calculated surface- and bulk-mode frequencies depends strongly on the particular characteristics of the shell model chosen for the bulk. Models which give nearly identical results for

the bulk dispersion curves can give considerably different results for the surface. With the available experimental data a choice between different bulk models cannot yet be made. It may therefore be necessary to rederive some of the model parameters when more surface data become available. Our aim here was to show that interesting dynamical effects happen at the surfaces of $SrTiO_3$, which merit further experimental investigations. Furthermore, the experimental study of surface modes will, in general, provide stringent criteria for a proper choice of bulk models.

Acknowledgments

This work was partially supported by the Robert A Welch Foundation through Grant No. F-433, and by a NATO Travel Grant. Acknowledgment is also made to the donors of the Petroleum Research Fund, administered by the American Chemical Society, for partial support of this research.

References

Bäuerle D, Wagner D, Wöhlecke M, Dorner B and Kraxenberger H 1980 *Z. Phys.* B **38** 335
Becher R 1989 *PhD Thesis* Universität Regensburg
Bickel N, Schmidt G, Heinz K and Müller K 1989 *Phys. Rev. Lett.* **62** 2009
Bilz H and Kress W 1979 *Phonon Dispersion Relations in Insulators (Springer Series in Solid State Sciences 10)* (Berlin: Springer)
Birnie III D P 1990 *J. Mater. Res.* **5** 1933
Bussmann A, Bilz H, Roenspiess R and Schwarz K 1980 *Ferroelectrics* **25** 343
Bussmann-Holder A, Bilz H, Bäuerle D and Wagner D 1981 *Z. Phys.* B **41** 353
Cowley R A 1964 *Phys. Rev.* A **134** 981
—— 1978 *Lattice Dynamics* ed M Balkanski (Paris: Flammarion) p 625
Cowley R A , Buyers W J L and Dolling G 1969 *Solid State Commun.* **7** 181
de Wette F W, Kress W, and Schröder U 1985 *Phys. Rev.* B **32** 4143
—— 1987 *Phys. Rev.* B **35** 2474
Heyen E T *et al* 1990 *Solid State Commun.* **74** 1299
Kress W, de Wette F W, Kulkarni A D, and Schröder U 1987 *Phys. Rev.* B **35** 5783
Kress W, Schröder U, Prade J, Kulkarni A D, and de Wette F W 1988 *Phys. Rev.* B **38** 2906
Kress W, Prade J, Schröder U, Kulkarni A D and de Wette F W 1989 *Physica* C **162-164** 1345
Kulkarni A D, de Wette F W, Prade J, Schröder U, and Kress W 1990 *Phys. Rev.* B **41** 6409
Kulkarni A D, Prade J, de Wette F W, Kress W and Schröder U 1989 *Phys. Rev.* B **40** 2642
Lines M E and Glass A M 1977 *Principles and Applications of Ferroelectric and Related Materials* (Oxford: Clarendon)
Migoni R, Rieder K H, Fischer K and Bilz H 1976 *Ferroelectrics* **13** 377
Prade J, Kulkarni A D, de Wette F W, Kress W, Cardona M, Reiger R and Schröder U 1987 *Solid State Commun.* **64** 1267
Prade J, de Wette F W, Kulkarni A D, Reiger R, Schröder U and Kress W 1988 *Surf. Sci.* **211/212** 329
Prade J, Kulkarni A D, de Wette F W, Schröder U and Kress W 1989 *Phys. Rev.* B **39** 2771
Prade J, Schröder U, Kress W, Kulkarni A D, and de Wette F W *Phonons 1989* ed S Hunklinger, W Ludwig and G Weiss (Singapore: World Scientific) ch 2, p 946
Reiger R, Prade J, Schröder U, de Wette F W, Kulkarni A D and Kress W 1989 *Phys. Rev.* B **39** 7938
Schröder U, Prade J, de Wette F W, Kulkarni A D, and Kress W 1990 *Superlatt. Microstruct.* **7** 247
Shirane G and Yamada Y 1969 *Phys. Rev.* **177** 858
Stirling W G 1972 *J. Phys. C: Solid State Phys.* **5** 2711
Stirling W G and Currat R 1976 *J. Phys. C: Solid State Phys.* **9** L519
Toennies J P and Vollmer R 1991 *Phys. Rev.* B **44** 9833
Wagner D, Bäuerle D, Schwabl F, Dorner B and Kraxenberger H 1980 *Z. Phys.* B **37** 317
Yamada Y and Shirane G 1969 *J. Phys. Soc. Japan* **26** 396